J Mater Sci (2008) 43:1094–1101
DOI 10.1007/s10853-007-2249-7

Characterization and dielectric properties of β-SiC nanofibres

Yiming Yao · Anna Jänis · Uta Klement

Received: 6 July 2007 / Accepted: 23 October 2007 / Published online: 4 December 2007
© Springer Science+Business Media, LLC 2007

Abstract SiC nanofibres produced by chemical vapour reaction technique are investigated using scanning and transmission electron microscopy. The nanofibres have been found to have a crystalline core of β-SiC sheathed with thorn-like turbostratic carbon or amorphous Si/O/C, respectively. For this material, real and imaginary part of relative permittivity is measured in a frequency range of 1–18 GHz at room temperature. The results reveal that the permittivity and dielectric loss in the SiC nanofibres are a magnitude higher compared with sub-microcrystalline SiC powder. Composition and nanostructure are held responsible for the difference in dielectric properties. The mechanisms of dielectric loss in the SiC nanofibres are discussed based on interfacial polarization, lattice defects in the SiC nanofibre cores and conduction loss of turbostratic carbon in the thorn-like sheath of SiC nanofibres.

Introduction

The discovery of carbon nanotubes (CNT) in 1990 has lead to far-reaching technological interest in one-dimensional SiC nanomaterials due to their excellent properties and promising applications in nanocomposites, nanoelectronics and nanomechanics [1–3]. SiC is one of the well-known materials with high temperature resistance, low density, high ductility and high strength. As the elastic modulus and strength of one-dimensional SiC nano materials are superior to those of bulk and micrometer-whisker counterparts, they are widely considered as reinforcements increasing strength and toughness [4–6]. On the other hand, SiC is a wide band gap semiconductor with unique physical/chemical stability, thermal conductivity and breakdown electric field. Therefore, SiC nanofibres and devices are expected to be used under harsh environments of high temperature, high power and high frequency [7, 8].

Up to now, research on SiC nanofibre materials was often directed towards electron field emission [9, 10], optics [11] and photoluminescence [12, 13]. Also advanced synthesis techniques were in the focus. However, only a few publications can be found on dielectric and microwave/infrared (IR) properties that are critical for high performance insulators, integrated circuits and dielectric applications. Recently, Kassiba et al. [14] have reported remarkable dielectric and conductive properties for SiC nanopowders. A detailed study is needed for obtaining fundamental knowledge in dielectric properties of SiC nanofibre materials.

In the present article, microstructures and relative permittivity properties of two kinds of β-SiC nanofibres produced with chemical vapour reaction technique are investigated, and the results are compared with commercial sub-microcrystalline β-SiC powder. Aim is to link the dielectric behaviour in a high frequency range to the microstructure/chemistry of SiC nanofibres in order to gain a better understanding on the mechanisms in dielectric properties and dielectric loss of SiC nanofibre materials.

Y. Yao (✉) · U. Klement
Materials and Manufacturing Technology, Chalmers University of Technology, Gothenburg 412 96, Sweden
e-mail: yiming.yao@chalmers.se

A. Jänis
Division of Sensor Systems, Swedish Defence Research Agency, Linkoping 581 11, Sweden

Experimental

Materials characterization

SiC nanofibres were produced at Laboratoire des Multimatériaux et Interfaces (LMI), University Claude Bernard in Lyon, France. The nanofibres were grown using direct synthesis technique, i.e. thermal treatment of commercial silicon particles disposed in a graphite crucible under N_2 atmosphere. Details about the synthesis technique can be found in [15] from LMI group. The two nanofibre samples were denoted as Sample-A and Sample-B, respectively. X-ray diffraction (XRD) was performed in a Bruker axs D8 ADVANCE diffractometer using Cr Kα radiation ($\lambda = 0.22897$ nm) with scanning speed of 0.05°/s. Microstructural characterization and chemical analysis were carried out using a Leo 1550 Gemini scanning electron microscope (FEG-SEM) equipped with energy-dispersive spectrometer (EDS), and a Zeiss 912 Omega transmission electron microscopy (TEM) with integrated energy filter and attached EDS detector, operating at 120 kV. The TEM specimens were prepared by dispersing the nanofibres in ethanol (ultrasonic bath), and depositing the suspension on a holey carbon film grid.

Permittivity measurement

A Wiltron 37269B vector network analyser was used to measure reflection in the frequency range of 1–18 GHz. The as-received SiC nanofibre material was packed into a compactor (7 mm in diameter) with a centre conductor (3 mm in diameter). The equipment was calibrated using a short, open and matched load-termination and empty shorted powder compactor as a phase reference. The relative measurement error for non-magnetic materials is around 1% for dielectric materials and 10% for conductive materials. Both real and imaginary parts of relative permittivity $\varepsilon_r = \varepsilon_r' + i\varepsilon_r''$ and relative permeability $\mu_r = \mu_r' + i\mu_r''$ (ε_r', ε_r'' and μ_r', μ_r'' are real and imaginary parts of relative permittivity and permeability, respectively) were calculated from the measured reflection coefficient [16]. For non-ferrite material, the complex part of permeability was taken as $\mu_r = 1 + i0$. In order to compare the dielectric properties of the SiC nanofibres and sub-microcrystalline SiC powder, the same measurements were performed for commercial SiC powder (SiC UF-25, Starck [17]) with an average particle size of 0.45 μm.

Results

Morphology and phase composition

The surfaces of the as-synthesised nanofibre bundles were covered by a "skin" (with a thickness about 0.5 mm) consisting of entangled fibres and foreign particles. The foreign particles were charging under the electron beam in the SEM due to low conductivity. When the skin was carefully removed using tweezers, pure and uniform nanofibres were exposed. Analysis has shown that the nanofibres inside the bundle contain C, Si and O with impurities of Al and Cl, whereas the scale contains higher oxygen and lower carbon contents compared with the inner part (Jänis et al., 2006, unpublished). Observations and analyses presenting in this study concern only those nanofibres in the centre parts of such fibre bundles. The average compositions estimated from measurements over a few mm^2 of the samples show that in Sample-A there is more than 50 at% C, while in Sample-B there is more than 40 at% O (Table 1). If we assume that O is stoichiometrically combined with Si as silica, and the residual Si is combined with C to form SiC, there would be about 45 at%

Table 1 EDS analysis from the inner parts of nanofibre bundles

	C (at%)	O (at%)	Si (at%)
Sample-A	51.3 ± 4.0	28.1 ± 3.6	20.7 ± 2.6
Sample-B	21.0 ± 2.2	40.3 ± 0.7	38.7 ± 2.2

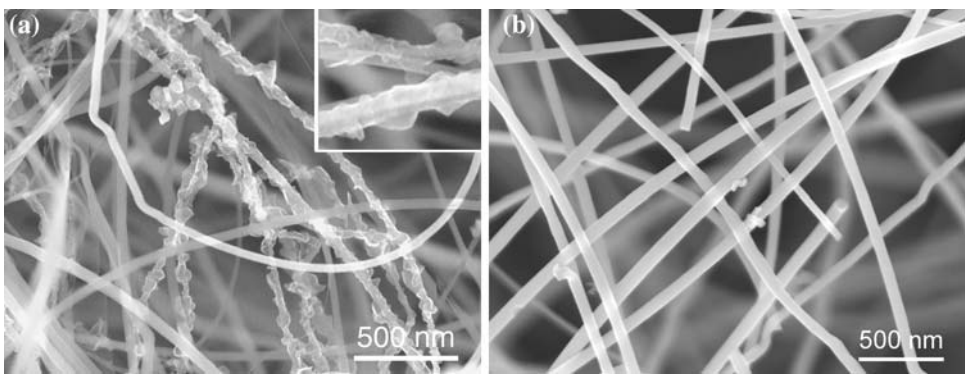

Fig. 1 FEG-SEM images of SiC nanofibre samples. (**a**) Sample-A contains nanofibres with rough surfaces of a thorn-like morphology. The insert shows a magnified image. (**b**) Nanofibres in Sample-B have smooth surfaces

free carbon in Sample-A, but no excess carbon in Sample-B. The SEM image in Fig. 1a shows that the nanofibres in Sample-A are around 60 nm in diameter and several hundreds of micrometer in length. About half of the nanofibres in this sample have a rough surface with a thorn-like morphology. In Sample-B, the nanofibres have an average diameter of about 80 nm and generally show a smooth surface (Fig. 1b).

The XRD diffractograms in Fig. 2 indicate the presence of amorphous constituents in the nanofibre samples. The reflections are identified as cubic β-SiC with a lattice parameter $a = 0.4349$ nm (JCPDS card No. 73-1665). The reflections located at $2\theta = 51.7$–$53.9°$ originate from the polytype structures of 6H–SiC and 15R–SiC. In Sample-A, a broadened peak centred at $2\theta = 39.4°$ is corresponding to the (002)-reflection of graphite with $a = b = 0.2470$ nm and $c = 0.6790$ nm (JCPCS card No. 75-1621). In terms of Scherrer-relation ($\Delta\theta(\text{rd}) \approx \lambda/L \cdot \cos\theta$; with L being grain size) and the experimental data of $\Delta\theta(\text{rd}) \approx 0.04$ rd at $\theta = 19.65°$ of graphite (002) reflection, the estimated grain size L in the graphite phase is 6.5 nm. There is no obvious evidence for crystalline silica in both samples; therefore, the substantial amount of O in the nanofibres revealed by SEM/EDS is assumed to come from the Si/O/C amorphous phase (to be proven by TEM analyses in next section).

TEM analyses

The zero-loss energy filtered TEM image in Fig. 3a shows the typical microstructure of the SiC nanofibres in Sample-B. The nanofibres have a nanocable structure, i.e. a crystalline core (presenting in diffraction contrast) covered by an amorphous outer layer. An enlarged image in Fig. 3b shows that a single nanofibre with the β-SiC core oriented at the [112] direction is covered with a 20 nm thick amorphous layer. Defects, e.g., stacking faults are frequently observed in the core of nanofibres in both samples, and closely spaced stacking faults are often found in the fibre growth direction. The streaks in the inserted selected area electron diffraction (SAED) pattern in Fig. 3c indicate that the stacking faults form parallel to β-SiC (111) planes oriented at the growth direction of the nanofibre. In Sample-A, nanofibres with both cabled and thorn-like structures are found (Fig. 3d). As can be seen in Fig. 3e, the nanofibres with thorn-like surface have a crystalline core-structure too. The corresponding SAED pattern in Fig. 3e reveals fragments of the ring pattern of (002) graphite planes with an interplanar spacing of $d_{(002)} = 0.342$ nm, which can be indexed with the superimposed [111] β-SiC pattern for calibration.

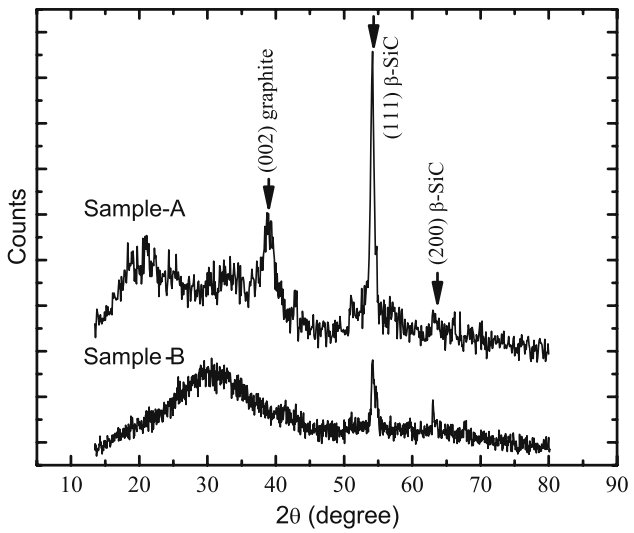

Fig. 2 XRD diffractograms of Sample-A and Sample-B

Energy-dispersive spectrometer line-profiles of C, O and Si are measured over the cross sections of nanofibres with thorn-like and smooth cabled surfaces. Only C, but no Si and O is presented in the thorn-like outer layer (Fig. 4a). In comparison, the profiles of Si, O and C are overlaid in the cable layer in the cabled nanofibre (Fig. 4b). The elemental profile of the cable layer does not show a well-defined interface. This implies that C is dissolved in the amorphous cable layer. Hence, it is amorphous Si/O/C, instead of amorphous silica, that is formed in the cable layer in the cabled nanofibres.

Fig. 5a shows EELS spectra from different nanofibres. Distinct ionisation edges of C-K (284 eV) and O-K (532 eV) are displayed in the spectra of nanofibres with cabled and thorn-like structure, while only the C-K edge appears in the spectrum of a non-cabled fibre containing stacking faults (see Fig. 3c). The relative composition expressed by the oxygen/carbon ratio (O/C) is determined using quantitative EELS. Since the EELS spectra are acquired from individual nanofibres with diameter of 80–150 nm, the multiple scattering in the spectrum is taken care of using de-convolution process, and the background is subtracted using power law. A high O level of O/C = 1.1–2.5 is observed in amorphous cabled nanofibres. The O/C value is found to increase with relative thickness $(R-r)/R$ of the cable sheath (with r being core radius and R fibre radius) (Fig. 5b). It means that O content in the cabled nanofibre is directly related to the relative volume of the cable layer. In contrast, the nanofibres with thorn-like surface morphology show a low O level (i.e. a high C level) of O/C = 0.17–1.0. The EELS measurements are consistent with the SEM/EDS results given in Table 1. Figure 5c shows the energy loss near edge spectrum (ELNES) at the C-K edge of nanofibres with the thorn-like and amorphous cabled structures. The graphite characteristic in the nanofibres with thorn-like structure is well defined by

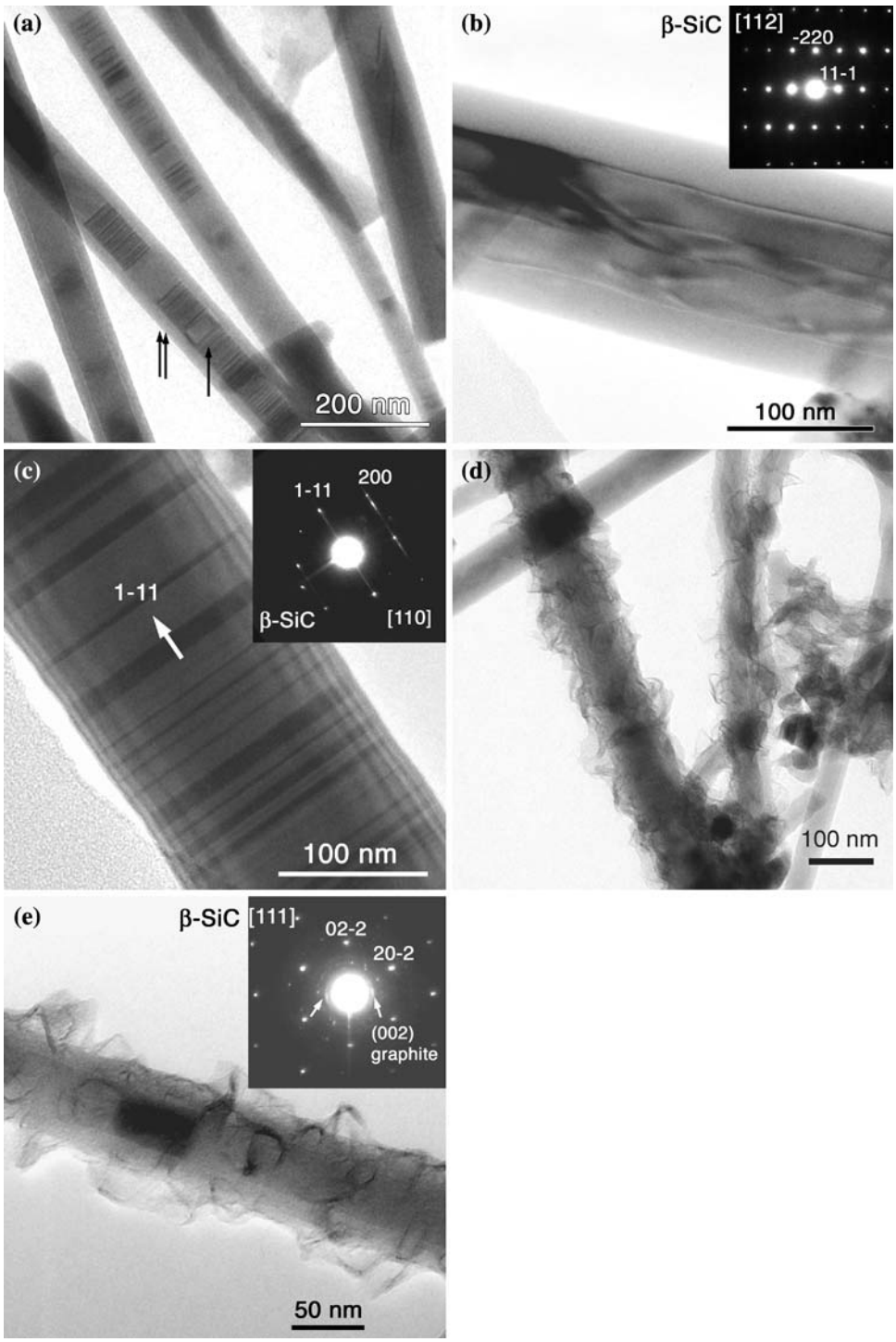

Fig. 3 Zero-loss TEM images from Sample-A and Sample-B. (**a**) Typical nanofibre structure in Sample-B. The crystalline core and amorphous layer are indicated by arrows. (**b**) A cabled fibber and the inserted micro-diffraction pattern from the β-SiC core. (**c**) Stacking faults in the fibber growth axis; the $\langle 111 \rangle$ direction is indicated as obtained by the inserted SAED pattern. (**d**) Typical nanofibre structure in Sample-A. (**e**) A thorn-like nanofibre with the respective SAED pattern, where the (002) diffraction ring from graphite are indicated by arrows

the π*-resonance at 285 eV, resulting from the sp^2 triple C=C bond in the basal plane. However, in the un-cabled and Si/O/C amorphous cabled nanofibres, the σ*-resonance at 290 eV predominates and the π*-edge signal is very weak. That means: a majority of C atoms both in the β-SiC crystalline core with a diamond structure and in the Si/O/C amorphous cable sheath has a tetrahedral sp^3 σ-bond that is basically localized between carbon and other atoms.

From the EDS line-profiles and ELNES measurements it can be concluded that the excess carbon in Sample-A is situated in the thorn-like outer layer which consists of turbostratic carbon [18], i.e. severely distorted graphene chains

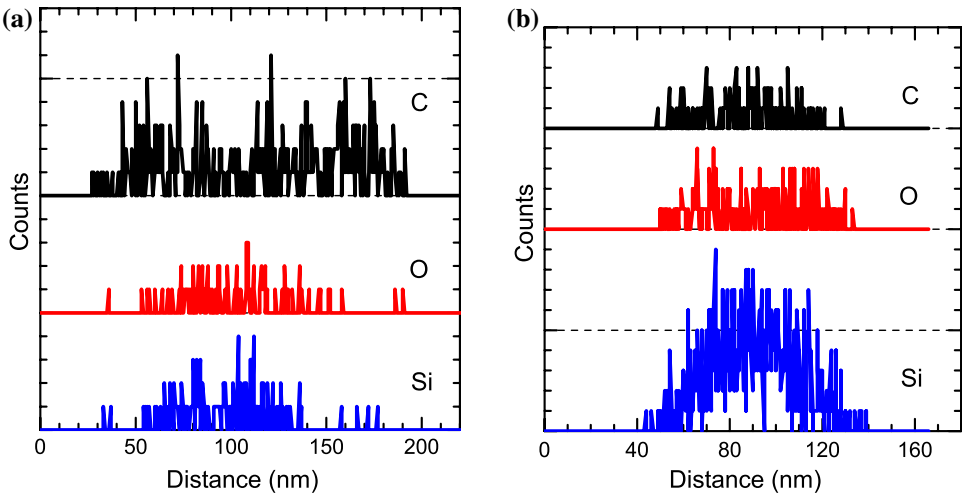

Fig. 4 EDS line-scan profiles of C, O and Si. (**a**) From a thorn-like nanofibre. (**b**) From a cabled nanofibre

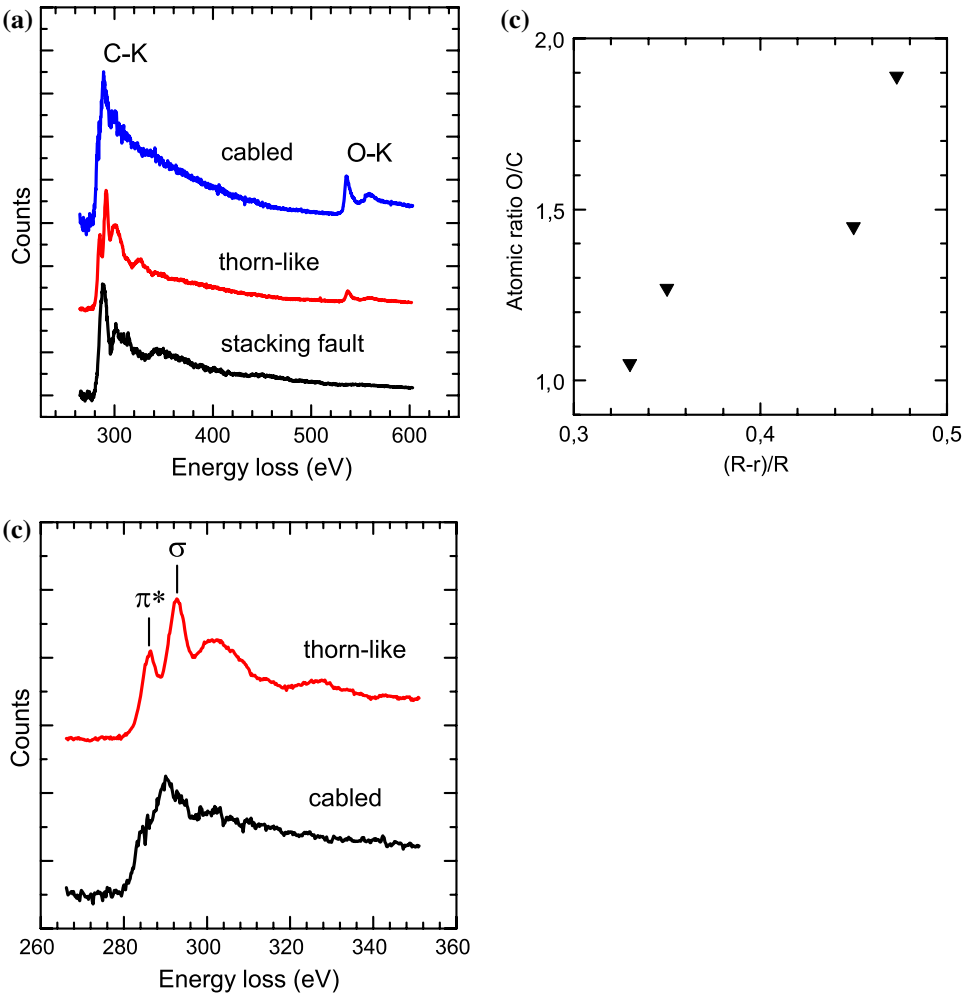

Fig. 5 EELS spectra from different nanofibres. (**a**) Distinct ionisation edges of C-K, (284 eV) and O-K (532 eV) are revealed in cabled and thorn-like nanofibres, but only the C-K edge appears in un-cabled stacking-faulted fibres. (**b**) Atomic ratio O/C dependence on $(R-r)/R$ (r is the radian of the core and R of the fibre) in the cable-structured nanofibres. (**c**) ELNES at C-K edge in thorn-like and cabled nanofibres

and planes instead of a three-dimensional graphite structure. While, most of the C-atoms in the Si/O/C cable layer form localized tetrahedral σ-bonds in the Si/O/C amorphous frameworks. Therefore, a lower electric conductivity can be expected along the Si/O/C amorphous cabled nanofibre compared to the turbostratic carbon sheathed nanofibre.

Permittivity

The relative complex permittivity can be describes as $\varepsilon_r(\omega) = \varepsilon(\omega)/\varepsilon_0 = \varepsilon_r'(\omega) + i\varepsilon_r''(\omega)$, where ω is the frequency of the impressed field and ε_0 is permittivity of vacuum; also the loss tangent $\tan\delta = \varepsilon_r''(\omega)/\varepsilon_r'(\omega)$ is frequency dependent [19]. Figure 6a–c provide the frequency dependences of $\varepsilon_r'(\omega)$, $\varepsilon_r''(\omega)$ and loss tangent $\tan\delta(\omega)$ in the three different samples at room temperature. As can be easily seen, the permittivity real and imaginary parts for the SiC nanofibre samples are significantly higher than those for the sub-microcrystalline SiC powder. In Sample-A, the $\varepsilon_r'(\omega)$ and $\varepsilon_r''(\omega)$ permittivity values decrease gradually with the frequency, whereas in Sample-B, $\varepsilon_r'(\omega)$ and $\varepsilon_r''(\omega)$ drop rapidly between 1 and 4 GHz and decrease slowly or remain nearly constant afterwards. In the sub-microcrystalline SiC powder, the dielectric loss tangent is very low over the whole measurement range owing to a low level of $\varepsilon_r''(\omega)$. In comparison, the average loss tangents in the two SiC nanofibre samples are one magnitude higher than that in the sub-microcrystalline SiC powder. Figure 6c also shows that the loss tangent of Sample-B is highest in the frequency range of 1–4 GHz, while between 6 and 13 GHz, the loss tangent in Sample-A is twice as high as in Sample-B.

Discussion

In a dielectric material, possible mechanisms for the polarization stimulated by an alternating electric field are (i) electron polarization, (ii) atomic polarization, (iii) reorientation (dipole) polarization and (iv) space-charge polarization [20]. Due to a large specific surface existing in nanomaterials, surface and interface effects play a critical role in dielectric relaxation and loss compared with conventional bulk/microcrystalline materials. Since the nanofibre samples were mechanically compacted for the permittivity measurements in this study, the material comprises a considerable amount of micro-porosity, vacancy clusters and dangling bonds. Distortions of the local electric field and of the space charge distribution takes place at these locations and a large number of dipole moments can be trapped there. Moreover, the SiC nanofibres in this study are heterogeneous materials, i.e., the SiC cores are sheathed by

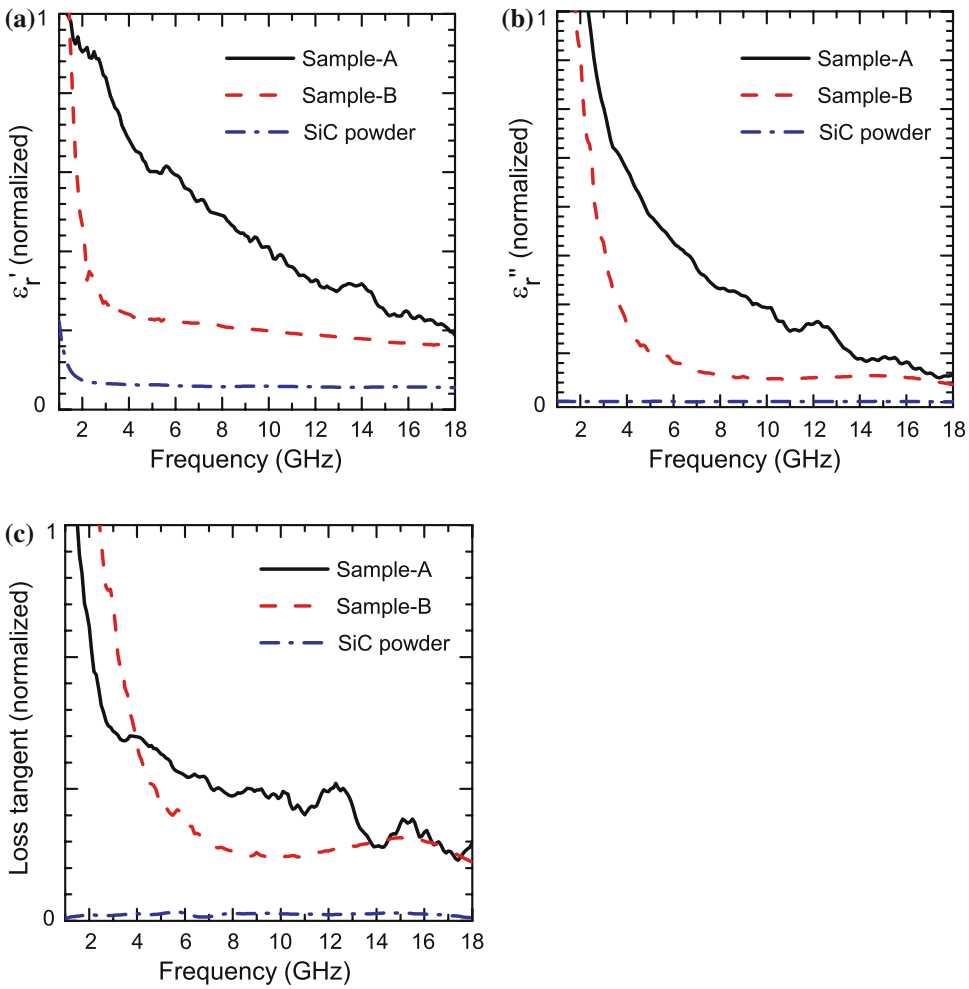

Fig. 6 Frequency dependence of relative permittivity of Sample-A, Sample-B and micro-crystalline SiC powder. (**a**) Real part $\varepsilon_r'(\omega)$. (**b**) Imaginary part $\varepsilon_r''(\omega)$. (**c**) Loss tangent $\tan\delta$

layers with different composition and structure. Charges might accumulate at the interface between the SiC core and the outer layer. According to the Maxwell–Wagner model [21], this interfacial polarization occurring in heterogeneous materials is indistinguishable from dipolar polarization at higher frequencies, and is likely to contribute to the dipolar relaxation and dielectric loss.

Kassiba et al. [22] have found that conductivity and dielectric properties of SiC nanopowders are correlated with the delocalised unpaired spins that are associated with the carbon-vacancies in the coexisting hexagonal α- and cubic β-SiC structure. Defects with charges can be attracted to these vacancies to form charged pairs or dipoles, as a result, energy dissipation occurs in presence of an external alternating electric field. A drastic increase in carbon-vacancy concentration is found when the particle size is in the range of 20–30 nm, which causes a corresponding rise in the relative permittivity in the SiC nanopowder [23, 24]. In both samples investigated in this study, numerous stacking faults have been observed on (111) planes in the β-SiC nanofibre cores. Stacking faults can be considered as interfaces between the hexagonal α- and the cubic β-SiC phases. This microstructural inhomogeneity might increase the carbon-vacancy concentration in the SiC crystalline cores, which, in turn, enhances the dielectric relaxation (in comparison, the sub-microcrystalline powders have a relatively lower concentration of lattice defects).

It is worthwhile to point out the influence of surface chemistry and structure of SiC nanofibres on the dielectric properties. The results from this study demonstrate that SiC nanofibres covered by thorn-like turbostratic carbon show superior values of permittivity and loss tangent compared with those having an amorphous Si/O/C cable layer. Charpentier et al. [24] have demonstrated that the excess carbon with π-bonding structure situated on the surface of SiC nanoparticles acts as channel barrier for hopping or tunnelling of charge carriers, and can lead to a major increase of the macroscopic permittivity of SiC nanopowder materials. Mouchon and Colomban [25] have reported that the high conductivity of a SiC long fibre reinforced composite results from the formation of carbon "crusts" at the fibre/matrix interface. At present stage, the permittivity data for turbostratic carbon and amorphous Si/O/C at high frequency are not available. Concerning direct conductivity, σ_{dc}, the intrinsic conductivity of turbostratic carbon black has a typical value of $\sigma_{dc} \approx 8 \times 10^{-4}$ $(\Omega\ \mathrm{cm})^{-1}$ (as an intrinsic semiconductor) [26], which is ascribed to a high charge carrier concentration originating from dangling sp^3-bonds and holes in sp^2-bonds in turbostratic carbon. The increased conductivity of macroscopic bundles of long multi-wall carbon nanotubes (MWNT) is about $\sigma_{dc} = 10^{-2}$ $(\Omega\ \mathrm{cm})^{-1}$ due to a long conjugation-length along graphite basal plane sheets in MWNT [27]. In contrast, the Si/O/C containing polymer (before carbon precipitates form in the polymer) exhibits a low conductivity level of $\sigma_{dc} \approx 10^{-11}$–$10^{-9}$ $(\Omega\ \mathrm{cm})^{-1}$ as an insulator [26]. Regarding the thickness (10–15 nm) of the outer layer on nanofibres, the electrical transport and conductive behaviour between the nanofibres are dominated by electron hopping or tunnelling of charge carriers through the interface barrier. In contrast, the conductivity in the outer layer along the nanofibres (with a length of several μm) can be estimated and compared to the relevant materials found by Cordelair and Greil [26], and Jin et al. [27]. Therefore, a higher effective loss factor that includes the conduction loss $(\sigma/(\varepsilon_{(}\omega))$ [28] could be gained from the higher conductivity in the turbostratic carbon sheath compared with that in the Si/O/C amorphous sheath. The difference in the dielectric loss between Sample-A and Sample-B can be attributed to the conduction-loss contribution.

Conclusion

The two investigated nanofibres consist of single crystalline β-SiC cores sheathed with outer layers of different morphologies and compositions. Sample-A has an outer layer of turbostratic carbon with thorn-like morphology, while Sample-B has a smooth surface and the nanofibres are covered with an amorphous Si/O/C cable layer. Stacking faults at (111) planes are often found perpendicular to the axis of the cubic β-SiC cores. The relative permittivity measurements reveal that $\varepsilon_r'(\omega)$, $\varepsilon_r''(\omega)$ and the loss tangent $\tan\delta(\omega)$ decrease with increasing frequency. In the high frequency range the permittivity real and imaginary parts for the SiC nanofibre samples are significantly higher than in the sub-microcrystalline SiC powder. The enhanced microwave response in the nanofibre samples compared with the microcrystalline powders is attributed to the interface polarization resulting from the high specific surface and defect concentration in the SiC nanocrystalline cores. Of the samples investigated in this study, Sample-A provides the highest permittivity. The difference in dielectric loss observed in the two nanofibre samples can be ascribed to the contribution of conduction-loss in the outer layer consisting of the π-bond turbostratic carbon.

Acknowledgements We would like to thank the Swedish Defence Nanotechnology Program for the financial support, and University Claude Bernard, Laboratoire des Multimatériaux et Interfaces (LMI) in Lyon, France, for the supply of the materials. We would also like to thank Jan Fagerström (Swedish Defence Research Agency) for helpful discussions.

References

1. Zhu Y, Kroto HW, Walton D, Lange H, Huczko A (2002) Chem Phys Lett 365:457
2. Yang W, Araki H, Kohyama A, Katoh Y, Hu Q, Suzki H (2004) J Nucl Mater 329–333:539

3. Zhang LD, Meng GW, Phillipp F (2000) Mater Sci Eng A 286:34
4. Petrovic JJ, Milewski JV, Rohr DL, Gac FD (1985) J Mater Sci 20:1167
5. Wong EW, Sheenhan PE, Lieber CM (1997) Science 277:1971
6. Kim Ph, Lieber CM (1999) Science 286:2148
7. Feng ZC, Mascerannas AJ, Choyke WJ, Powell JA (1988) J Appl Phys 64(6):3176
8. Fissel A, schröter B, Richer W (1995) Appl Phys Lett 66:3182
9. Bonard J-M, Salvetat J-P, Stocki T, de Heer WA, Forro L, Chatelain A (1998) Appl Phys Lett 73:918
10. Ryu YH, Park BT, Song YH, Yong K (2004) J Cryst Growth 271:99
11. Han WQ, Fan SS, Li QQ, Gu BL, Yu DP (1997) Chem Phys Lett 265:374
12. Feng DH, Jia TQ, Li XX, Xu ZZ, Chen J, Deng SZ, Wu ZS, Xu NS (2003) Solid State Commun 128:295
13. Liang CH, Meng GW, Zhang LD, Wu YC, Cui Z (2000) Chem Phys Lett 329:323
14. Kassiba A, Tbellout M, Charpentier S, Herlin N, Emery JR (2000) Solid State Commun 115:389
15. Saulig-Wenger K, Cornu D, Chassagneux F, Ferro G, Epicier Th, Miele Ph (2002) Solid State Commun 124:157
16. Weir WB (1974) Proc IEEE 62:33
17. Starck HC (2006) Home page: http://www.hcstarck.com. Accessed 01 Nov 2006
18. Charpentier S, Kassiba A, Bulou A, Monthioux M, Carchetier M (1999) Eur Phys J Appl Phys 8:111
19. Kassiba A (2003) In: Legrand AP, Sénémaud Ch (eds) Nanostructured silicon-based powders and composites. Taylor & Francis Group, London and New York, p 227
20. Kingery WD, Boven HK, Uhlmann DR (1976) Introduction to ceramics. John Wiley & Sons, New York, p 921
21. Raju GG (2003) Dielectrics in electric fields. Marcel Dekker, Inc., New York, Basel. http://www.engnetbase.com. Accessed 6 Dec 2006
22. Kassiba A, Charpentier S (2003) In: Legrand AP, Sénémaud C (eds) Nanostructured silicon-based powders and composites. Taylor & Francis, London and New York, p 211
23. Kityk IV, Kassiba A, Tuesu K, Charpentier C, Ling Y, Makowska-Janusik M (2000) Mater Sci Eng B 77:147
24. Charpentier S, Kassiba A, Emery J, Cauchetier M (1999) J Phys Condens Mater 11:4887
25. Mouchon E, Colomban Ph (1996) J Mater Sci 31:323
26. Cordelair J, Greil P (2000) J Eur Ceram Soc 20:1947
27. Jin R, Zhou ZX, Mandrus D, Ivanov IN, Eres G, Howe JY, Puretzky AA, Geohegan DB (2007) Phys B 388:326
28. Priou A (1992) Dielectric properties of heterogeneous materials, Pier 6 progress in electromagnetics research. Elsevier, New York, p 14